Original Article

Novel Insights into the Aortic Mechanical Properties of Mice Modeling Hereditary Aortic Diseases

Nicolo Dubacher, Kaori Sugiyama, Jeffrey D. Smith, Vanessa Nussbaumer, Máté Csonka, Szilamér Ferenczi, Krisztina J. Kovács, Sylvan M. Caspar, Lisa Lamberti, Janine Meienberg, Hiromi Yanagisawa*, Mary B. Sheppard*, Gabor Matyas*

Affiliations

Center for Cardiovascular Genetics and Gene Diagnostics, Swiss Foundation for People with Rare Diseases, Switzerland (N.D., V.N., M.C., S.M.C., L.L., J.M., G.M.), Translational Cardiovascular Technologies, Department of Health Sciences, ETH Zurich, Switzerland (N.D.), Institute for Advanced Research of Biosystem Dynamics, Research Institute for Science and Engineering, Waseda University, Japan (K.S.), Life Science Center for Survival Dynamics, Tsukuba Advanced Research Alliance, University of Tsukuba, Japan (K.S., H.Y.), Saha Cardiovascular Research Center, University of Kentucky, USA (J.D.S.), Heart and Vascular Center, Semmelweis University, Hungary (M.C.), Laboratory of Molecular Neuroendocrinology, Institute of Experimental Medicine, Hungary (S.F., K.J.K.), Department of Family and Community Medicine, University of Kentucky, USA (M.B.S.), Saha Aortic Center, University of Kentucky, USA (M.B.S.), and Zurich Center for Integrative Human Physiology, University of Zurich, Switzerland (G.M.).

*H. Yanagisawa, M.B. Sheppard, and G. Matyas are joint senior authors.

Short title: Aortic Rupture Force in Mice Modeling Aortic Diseases

Correspondence to: Gabor Matyas, PhD, Center for Cardiovascular Genetics and Gene Diagnostics, Swiss Foundation for People with Rare Diseases, 8952 Schlieren-Zurich, Switzerland. Email matyas@genetikzentrum.ch, Phone +41-43-433-86-86

ABSTRACT

OBJECTIVE: Hereditary aortic diseases (hADs) increase the risk of aortic dissections and ruptures. Recently, we have established an objective approach to measure the rupture force of the murine aorta, thereby explaining the outcomes of clinical studies and assessing the added value of approved drugs in vascular Ehlers-Danlos syndrome (vEDS). Here, we applied our approach to six additional mouse hAD models.

APPROACH AND RESULT: We used two mouse models of Marfan syndrome (MFS) as well as one smooth-muscle-cell-specific knockout (SMKO) of *Efemp2* and three CRISPR/Cas9-engineered knock-in models (*Ltbp1*, *Mfap4*, and *Timp1*). Moreover, one of the two MFS models was subjected to 4-week-long losartan treatment. Per mouse, three rings of the thoracic aorta were prepared, mounted on a tissue puller, and uniaxially stretched until rupture. The aortic rupture force of the SMKO and both MFS models was significantly lower compared with wild-type mice but in both MFS models higher than in mice modeling vEDS. In contrast, the *Ltbp1*, *Mfap4*, and *Timp1* knock-in models presented no impaired aortic integrity. As expected, losartan treatment reduced aneurysm formation but surprisingly had no impact on the aortic rupture force of our MFS mice.

CONCLUSIONS: We demonstrate for the first time that our read-out system is able to characterize the aortic biomechanical integrity of mice modeling not only vEDS but also related hADs, allowing the aortic-rupture-force-focused comparison of mouse models. Furthermore, aneurysm progression alone may not be a sufficient read-out for aortic rupture, as blood-pressure-lowering therapies preventing aortic aneurysms might not strengthen the weakened aortic wall. These results may contribute to better medical therapies of hADs.

Key Words: aortic aneurysm, dissection, rupture, biomechanical integrity, *Efemp2*, *Fbn1*, Marfan syndrome

57 **Nonstandard Abbreviations and Acronyms**

hAD(s)	hereditary aortic disease(s)
AGTR1	angiotensin II receptor type 1
Bgn	biglycan (encoding gene in mice)
ECM	extracellular matrix
Efemp2	fibulin-4 (Fbln4) (encoding gene in mice)
Fbn1	fibrillin-1 (encoding gene in mice)
Ltbp1	latent TGF-β binding protein 1 (encoding gene in mice)
Mfap4	microfibril associated protein 4 (encoding gene in mice)
MFS	Marfan syndrome
MMP	matrix metalloproteinase
SMKO	smooth-muscle-specific knockout ($Efemp2^{loxP/KO};SM22\text{-}Cre^{Tg/Tg}$)
TAA(s)	thoracic aortic aneurysm(s)
TGF	transforming growth factor
Timp1	tissue inhibitor of matrix metalloproteinase 1 (encoding gene in mice)
vEDS	vascular Ehlers-Danlos syndrome

58

59 Hereditary aortic diseases (hADs) with life-threatening aneurysms and dissections are
60 associated with high morbidity and mortality and are the cause for up to ~2% of all deaths in
61 the Western world.[1] Syndromic and non-syndromic forms of hADs are rare (i.e., prevalence
62 <1:2000) but several forms have been identified so far. Despite considerable phenotypic
63 similarity, disease management can profoundly differ depending on the disease-underlying
64 gene(s) and, thus, molecular genetic testing is required to identify (likely) pathogenic
65 sequence variant(s) in hAD-associated genes.[2,3] The advent of high-throughput sequencing
66 has enabled genetic data generation at hitherto unprecedented scale, allowing for novel
67 insights into the molecular etiology of hereditary (aortic) diseases but requiring a high level of
68 expertise for appropriate data analysis and variant interpretation.[4] Currently, at least 50 genes

69 have been associated with hereditary thoracic aortic aneurysms (TAAs) and classified based
70 on the strength of association.[5] However, these genes cannot explain all the cases of heritable
71 TAAs, suggesting the presence of additional genes which, when mutated, may be causative
72 for hADs.[6]

73 Changes in the structural components of the extracellular matrix (ECM) as well as in
74 chemical and mechanical stimuli can influence the molecular signaling pathways that regulate
75 aortic wall homeostasis. Accordingly, hAD-causing sequence variants (mutations) can affect
76 the proper ECM organization, thereby directly impacting the mechanical properties of the
77 aorta as well as the mechanoregulation of vascular smooth muscle cells and their ability to
78 sense matrix-mediated mechanical stimuli.[7] This can result in an impaired aortic integrity and
79 mechanical functionality causing progressive weakening of the aortic wall, ultimately leading
80 to arterial dissection and/or rupture.[8] The mechanical properties of the thoracic aorta can be
81 derived from *in vivo* imaging parameters such as aortic wall distensibility and local pulse
82 wave velocity or, especially aortic rupture, studied directly in *ex vivo* aortic samples.[9-11] In
83 humans, however, studies assessing the clinically highly relevant rupture (with or without
84 aneurysm/dissection) of the thoracic aorta in hAD are significantly limited. Thus, non-human
85 models harboring (likely) disease-causing mutations in candidate or already established hAD-
86 associated gene(s) are the (only) alternative in combination with an appropriate read-out at
87 individual level.

88 Recently, we have established an objective approach to measure the aortic rupture
89 force (maximum tensile force) of uniaxially stretched murine thoracic aortic rings as read-out
90 for the biomechanical integrity of the aorta.[12] We have used this approach to clarify whether
91 or not antihypertensive drugs may have an additional benefit (added value) to strengthen the
92 weakened thoracic aorta (drug repurposing). Indeed, we showed that celiprolol, a 3rd-
93 generation β-blocker, can improve the biomechanical integrity of the aortic wall (i.e., beyond
94 the β-blocker-typical prevention of rise in blood pressure and heart rate),[12] explaining the

95 outcomes of clinical and retrospective studies in vascular Ehlers-Danlos syndrome (vEDS,
96 OMIM #130050).[13-15] This added value of celiprolol, however, cannot simply be extrapolated to
97 other β-blockers, as we have demonstrated for bisoprolol using aortic rupture force as read-out.[16]

98 Here, we applied our established read-out approach[12] to measure the aortic rupture
99 force in six additional mouse hAD models and compared their aortic rupture force with that of
100 vEDS mice: (i) We used the two most widely investigated mouse models of Marfan syndrome
101 (MFS, OMIM #154700) (*Fbn1*^{C1041G} and *Fbn1*^{mgR}),[17-19] a rare autosomal-dominant inherited
102 disease with severe cardiovascular manifestations, such as TAAs predisposing to aortic
103 dissection and rupture, caused by mutations in the gene encoding fibrillin-1 (*FBN1* in
104 humans, *Fbn1* in mice).[20] In one of the two mouse MFS models (*Fbn1*^{mgR}), we also aimed to
105 clarify whether or not the frequently prescribed angiotensin-II-receptor-type-1 (AGTR1)
106 inhibitor losartan, which has been shown to slow down aneurysm progression in MFS,[21-25]
107 also strengthens the potentially weakened thoracic aorta. (ii) Furthermore, we assessed the
108 aortic rupture force in an *Efemp2* (encoding fibulin-4 [Fbln4]) smooth-muscle-specific knock-
109 out (SMKO) model recapitulating key vascular phenotypic features (aortic aneurysms and
110 arterial tortuosity)[26] of the autosomal-recessive inherited connective tissue disorder cutis laxa
111 type 1B (OMIM #614437).[27,28] (iii) Moreover, we used three novel CRISPR/Cas9-engineered
112 knock-in models (*Ltbp1*^{G1132S}, *Mfap4*^{D42A}, *Timp1*^{I120T}) to assess the causality of human-
113 equivalent variants in hAD candidate genes detected by whole-genome sequencing (WGS).[6]

114

115 # METHODS

116 **Mouse strains**

117 In this study, multiple mouse strains were used. An overview can be found in the Major
118 Resources Table in the Supplemental Material. Wild-type mice are referred to as $^{+/+}$.

119

120 ***Fbn1^{C1041G}* and *Fbn1^{mgR}* Mouse Models**

121 For the *Fbn1^{C1041G}* mouse model (C57BL/6J background), 10-week-old heterozygous
122 (*Fbn1$^{+/C1041G}$*, n=10) and wild-type (*Fbn1$^{+/+}$*, n=10) mice were ordered in frozen condition
123 from Jackson Laboratory (JAX stock #012885, Bar Harbor, ME, USA). Tail biopsies were
124 taken to confirm the genotypes of delivered mice, for which DNA extraction, PCR and
125 subsequent Sanger sequencing were performed as previously described.[12,17]

126 *Fbn1^{mgR}* mice (C57BL/6J background) were bred and maintained on a 14/10-hour
127 light/dark cycle receiving standard rodent chow and water *ad libitum*. Mice were genotyped
128 as described elsewhere.[18] In addition, 4-week-old homozygous (*Fbn1$^{mgR/mgR}$*, n=12) and wild-
129 type (*Fbn1$^{+/+}$*, n=10) mice were treated for 4 weeks with losartan dissolved in drinking water
130 at a concentration of 600 mg/L (LTK Labs, St. Paul, MN, USA, ~180 mg/kg bodyweight per
131 day), whereas age-matched untreated *Fbn1$^{mgR/mgR}$* (n=17) and *Fbn1$^{+/+}$* (n=10) littermates
132 receiving normal drinking water served as controls. Animals were weighed at the beginning
133 and at the end of the treatment and water consumption was monitored regularly to ensure that
134 control and treated mice drank comparable quantities. At the end of the treatment, mice were
135 euthanized using CO_2 and subsequently frozen. Treatment protocols were approved by the
136 University of Kentucky IACUC (approval reference number: 2016-2437) in line with the
137 local guidelines.

138

139 ***Efemp2* SMKO Model**

140 *Efemp2*$^{loxP/KO}$;*SM22-Cre*$^{Tg/Tg}$ (SMKO) and wild-type littermates (wild-type for *Efemp2* but
141 containing the SM22α-Cre transgene, *Efemp2*$^{+/+}$;*SM22-Cre*$^{Tg/Tg}$) with a mixed genetic
142 background (C57BL/6J; 129SvEv) were bred and maintained on a 12-hour light/dark cycle
143 receiving standard rodent chow and water *ad libitum*. Genotyping was performed as
144 previously described.[26] Wild-type (n=11) and SMKO (n=11) littermates were euthanized with
145 CO_2 at 8 weeks of age and subsequently frozen. Animal experimentation and maintenance
146 were in accordance with and approved by the Institutional Animal Experiment Committee of
147 the University of Tsukuba, Japan (approval reference number: 21-108).

148

149 **CRISPR/Cas9-Engineered Mouse Models**

150 Three CRISPR/Cas9 knock-in mouse models (*Ltbp1*^{emG1132S}, *Mfap4*^{emD42A}, and *Timp1*^{emI120T})
151 were generated on the C57BL/6NJ background by Cyagen (Santa Clara, CA, USA), thereby
152 introducing human-equivalent sequence variants detected in our WGS cohort of hAD patients
153 (GRCm38/mm10 chr17(Ltbp1):g.75,315,062G>A, chr11(Mfap4):g.61,486,071A>C, and
154 chrX(Timp1):g.20,873,395T>C, modeling human variants *LTBP1* NM_206943.4: c.3418G>A
155 p.(Gly1140Ser), *MFAP4* NM_001198695.2: c.191A>C p.(Asp64Ala), and *TIMP1*
156 NM_003254.3: c.356T>C p.(Ile119Thr), respectively). Founder mice of the three strains were
157 bred and maintained on a 12-hour light/dark cycle receiving standard rodent chow and water
158 *ad libitum*. The genotype was determined after weaning at the age of 4 weeks by PCR and
159 subsequent Sanger sequencing using genomic DNA extracted of ear biopsies as previously
160 described.[12] Primers used for PCR and sequencing are listed in Table S1. One-year-old
161 heterozygous (*Ltbp1*$^{+/G1132S}$, n=10; *Mfap4*$^{+/D42A}$, n=10; *Timp1*$^{+/I120T}$, n=7), homozygous
162 (*Ltbp1*$^{G1132S/G1132S}$, n=10; *Mfap4*$^{D42A/D42A}$, n=8; *Timp1*$^{I120T/I120T}$, n=5), and hemizygous
163 (*Timp1*$^{0/I120T}$, n=9) mice as well as age-matched wild-type littermates serving as controls
164 (*Ltbp1*$^{+/+}$, n=10; *Mfap4*$^{+/+}$, n=9; *Timp1*$^{+/+}$, n=8) were euthanized with CO_2 and subsequently

165 frozen (cf. one-year-old mice were used to be able to detect any late-onset effects of the
166 variants). Animal experimentation and maintenance were in accordance with institutional and
167 local guidelines (approval reference number: ZH107/17, Zurich, Switzerland) conforming to
168 the EU Directive 2010/63/EU for animal experiments.
169

170 **Aortic Rupture Force Measurements**

171 Euthanized mice kept in a frozen state were thawed immediately before measurement of
172 aortic rupture force. For all mouse models, the maximum tensile force at rupture (in mN) of
173 three uniaxially stretched 1.5-mm thoracic aortic rings/segments (segment S1, ascending
174 aorta, after heart; segment S2, descending aorta, after aortic arch; segment S3, descending
175 aorta, adjacent to S2) per mouse was measured and relative rupture force was calculated by
176 setting the arithmetic mean of the respective wild-type S1 to 100% as previously described.[12]
177 For the SMKO and both MFS models, the stretching positions of the tissue puller until both 5
178 mN (load-free aortic diameter) and maximum force (rupture of aortic segment) were
179 determined (in µm) as moved distance of the mounting pins during stretching. Mice were
180 randomized and all measurements were performed blinded for the investigator.
181

182 **Statistical Analyses**

183 For arithmetic means, 95% confidence intervals (CIs) were calculated using two-tailed critical
184 values of *t*-distribution (vassarstats.net/conf_mean.html). For means with non- or slightly
185 (<2% of means) overlapping 95% CIs compared in the text, two-tailed *P* values were
186 calculated by two-sample *t*-test (equal sample variances according to *F*-test) or Welch's *t*-test
187 (unequal sample variances according to *F*-test), assuming normal distribution of independent
188 samples (vassarstats.net/tu.html). For proportions, 95% CIs were calculated with continuity
189 correction (vassarstats.net/prop1.html). For additional information, see Supplemental Material.

190 # RESULTS

191 ## *Fbn1*^{C1041G} Mouse Model

192 Compared to *Fbn1*$^{+/+}$ mice, the aortic rupture force of *Fbn1*$^{+/C1041G}$ mice was significantly
193 decreased in all three aortic segments (S1, S2, and S3) (Figure 1A; Table S2). No significant
194 difference between *Fbn1*$^{+/+}$ and *Fbn1*$^{+/C1041G}$ mice was observed in the stretch at both 5 mN
195 (aortic diameter) and maximum force (aortic rupture) in all three aortic segments (Figure 1B;
196 Tables S3 and S4). Differences and trends in the relative aortic rupture force and stretch
197 values of *Fbn1*$^{+/+}$ and *Fbn1*$^{+/C1041G}$ mice were comparable in both sexes (Figure S1).

198

199 ## *Fbn1*^{mgR} Mouse Model

200 During losartan treatment, the mortality rate of treated *Fbn1*$^{mgR/mgR}$ mice (8.3% [95% CI,
201 0.4%-40.2%]) was not significantly lower than that of untreated *Fbn1*$^{mgR/mgR}$ mice (11.8%
202 [95% CI, 2.1%-37.7%]), while no wild-type mouse died (Figure 2A). Although on average
203 males were heavier than females, the body weight within sexes was not significantly different
204 before treatment (at the age of 4 weeks), but after treatment (at the age of 8 weeks)
205 *Fbn1*$^{mgR/mgR}$ males (especially losartan-treated) were noticeably heavier compared to wild-
206 type males (Figure 2B).

207 Compared with untreated *Fbn1*$^{+/+}$ mice, the aortic rupture force was significantly
208 decreased in all three aortic segments of both untreated and losartan-treated *Fbn1*$^{mgR/mgR}$ mice,
209 i.e., losartan did not strengthen the weakened aortic wall of *Fbn1*$^{mgR/mgR}$ mice modeling MFS
210 (Figure 3A; Table S5). Rather, the aortic rupture force of losartan-treated *Fbn1*$^{+/+}$ mice
211 tended to be reduced compared to untreated *Fbn1*$^{+/+}$ mice in all three aortic segments
212 measured, which requires further investigation (Figure 3A; Table S5).

213 The stretch of aortic segment S1 at both 5 mN (aortic diameter) and maximum force
214 (rupture) was significantly increased in untreated female and male *Fbn1*$^{mgR/mgR}$ mice
215 compared to untreated *Fbn1*$^{+/+}$ females and males, respectively, being the most pronounced in

216 males (Figure 3B; Tables S6 and S7). While losartan treatment of *Fbn1*$^{+/+}$ mice had no effect
217 on the stretch of S1 neither in female nor in male animals (Figure 3B; Tables S6 and S7),
218 losartan treatment considerably reduced the stretch of S1 at both 5 mN and maximum force in
219 both female and male *Fbn1*$^{mgR/mgR}$ mice (Figure 3B; Tables S6 and S7). In S2 and S3,
220 however, there were no considerable differences in the stretch at 5 mN and maximum force
221 (data not shown).
222
223 ***Efemp2* SMKO Mouse Model**
224 Compared with wild-type mice, our measurements showed significantly reduced relative
225 aortic rupture force in the ascending thoracic aorta (S1) but no difference in the descending
226 aorta (S2 and S3) of SMKO mice (Figure 4A; Table S8). Furthermore, in SMKO mice the
227 stretch at both 5 mN and maximum force was significantly higher in the ascending aorta (S1)
228 but significantly lower in the descending aorta (S3) at maximum force (Figure 4B; Tables S9
229 and S10).
230
231 ***Ltbp1*, *Mfap4*, and *Timp1* CRISPR/Cas9 Knock-In Mouse Models**
232 During the one-year period of aging, no *Ltbp1*, *Mfap4* or *Timp1* CRISPR/Cas9 knock-in mice
233 died due to aortic rupture. Moreover, the rupture force of the aortic segments S1, S2, and S3
234 showed no considerable difference between wild-type controls and hetero-, homo-, or
235 hemizygous mice of *Ltbp1*, *Mfap4*, and *Timp1* CRISPR/Cas9 knock-in mice (Figure 5; Table
236 S11).
237
238

239 **DISCUSSION**

240 Inbred mouse hAD models are valuable tools for the investigation of medical therapeutic
241 approaches and the establishment of gene-disease association and have been widely adopted
242 for the identification of cardiovascular abnormalities by assessing aortic diameter,
243 morphology, and wall thickness as well as by considering histological staining, omics data, or
244 survival rate.[29-33] Although these methods provide observational insights, they cannot
245 directly/objectively reveal how medical therapy or sequence variant(s) influences the strength
246 (i.e., rupture force) of the aortic wall and whether or not there is a risk for aortic dissection
247 and rupture. In this study, by measuring the aortic rupture force we provide hitherto
248 unprecedented insights into the aortic biomechanical integrity of three established
249 (*Fbn1*^{C1041G}, *Fbn1*^{mgR}, and *Efemp2* SMKO) and three novel candidate-gene (*Ltbp1*, *Mfap4*,
250 and *Timp1*) mouse hAD models.

251 By applying the aortic rupture force measurement to both mouse MFS models (i.e., the
252 phenotypically milder heterozygous *Fbn1*^{C1041G} and the phenotypically more severe
253 homozygous *Fbn1*^{mgR} mice), we showed for the first time a significantly decreased rupture
254 force as indicator for an impaired biomechanical integrity in the thoracic aorta, especially in
255 the ascending aorta (Figures 1A and 3A). Even though the aortic wall of *Fbn1*$^{+/C1041G}$ mice is
256 normal in appearance until about 3 months of age and only later on shows medial thickening
257 and/or progressive deterioration within the medial layer, including elastic fiber fragmentation
258 in association with excess expression of matrix metalloproteinase 2 (MMP2) and 9 (MMP9),
259 our read-out system allowed the identification of an impaired aortic wall integrity already at
260 an early stage compared to previously described methods (cf. *Fbn1*$^{+/C1041G}$ mice used in this
261 study were 10-week-old).[17,18]

262 In *Fbn1*$^{mgR/mgR}$ mice, treatment with the AGTR1-inhibitor losartan has been shown to
263 improve survival only before aneurysm development but not after.[34,35] In our study, survival
264 of *Fbn1*$^{mgR/mgR}$ mice treated with losartan was not improved, despite treatment start already at

265 the age of 4 weeks (Figure 2A). However, as the average survival of *Fbn1*$^{mgR/mgR}$ mice is just
266 below 16 weeks of age,[18] our treatment may be too short to conclusively evaluate the effect of
267 losartan on average survival. Regarding weight, survived 8-week-old *Fbn1*$^{mgR/mgR}$ males
268 (especially those treated with losartan) were heavier than wild-type males (Figure 2B), which
269 is unexpected considering the human MFS phenotype but has been observed previously in
270 this mouse model and is attributed to altered adipose tissue homeostasis.[36]

271 Furthermore, compared to untreated wild-type controls, in *Fbn1*$^{mgR/mgR}$ mice there was
272 a significantly increased stretch until both 5 mN (i.e., diameter) and maximum force (i.e.,
273 rupture) in the ascending aorta (Figure 3B), reflecting aneurysm development and confirming
274 macroscopic evaluation. These differences were even more pronounced in male than in
275 female mice, which is in line with previously published data using ultrasound
276 measurements.[37-38] Indeed, sex is a well-known risk factor for cardiovascular diseases and
277 several clinical studies have shown that sex also strongly influences the outcome of MFS,
278 with men having a higher risk for aortic dilatations and arterial events.[39-41]

279 Treatment of *Fbn1*$^{mgR/mgR}$ mice with losartan recognizably reduced stretch and, thus,
280 aneurysm formation (Figure 3B). Despite preventing aneurysm formation by likely reducing
281 blood pressure (as previously shown for the same dosage of losartan in the *Fbn1*^{C1041G} mouse
282 model),[21] losartan treatment did not impact the aortic rupture force and, hence, in case of
283 blood pressure spikes or continuously elevated blood pressure (e.g., upon discontinuation of
284 antihypertensive drug therapy), the vessel is still prone to rupture. This suggests that for the
285 investigation of potential medical therapeutic approaches in mouse hAD models presenting
286 with aneurysms, the sole prevention of aneurysm formation or the reduction of aneurysm
287 progression is not an adequate read-out for the strength of aortic wall. Thus, our read-out
288 system acts as a clinically relevant approach allowing novel insights into the evaluation of
289 medical therapies for the prevention of arterial events in hADs.

290 Moreover, the significantly reduced aortic rupture force demonstrated here indicates
291 that the absence of Fbln4 in the aortic ECM leads to an impaired aortic integrity in the
292 ascending aorta (Figure 4A). This is likely caused by the previously described profound
293 impact of the absence of Fbln4 on elastogenesis[42] and collagen biosynthesis,[26] also involved
294 in the development of ascending aortic aneurysms.[43,44] Accordingly, our measurements of
295 significantly increased aortic stretch reflected the aneurysm formation of the ascending aorta
296 of SMKO mice. Considering that the ascending aorta has the highest hemodynamic stress
297 burden in terms of pulse dampening (consistent with the highest elastin content),[45,46] it is
298 coherent that knock-out of *Efemp2* in vascular smooth muscle cells has the more pronounced
299 effect on the ascending aorta (i.e., S1 compared to S2 and S3).

300 In comparison to a previously reported mouse vEDS model (*Col3a1*^{m1Lsmi}),[12,16] the
301 relative aortic rupture forces of both *Fbn1*$^{+/C1041G}$ and *Fbn1*$^{mgR/mgR}$ mouse MFS models were
302 significantly higher in all three aortic segments (Figure 6; Table S12). The weaker thoracic
303 aorta of *Col3a1*$^{+/m1Lsmi}$ mice is also reflected, for example, in the higher mortality rate
304 compared with *Fbn1*$^{mgR/mgR}$ mice (Figure S2). In contrast, SMKO mice showed in the
305 ascending aorta (S1), where the aneurysms occurred, relative aortic rupture force values
306 comparable to or lower than those of mice modeling vEDS, while in the descending aorta (S2
307 and S3) with normal diameter the relative rupture force of SMKO mice was comparable to
308 that of mice modeling MFS (Figure 6; Table S12).

309 Because our measurements were able to reveal the reduced aortic rupture force of
310 established hAD mouse models as demonstrated here (*Fbn1*^{C1041G}, *Fbn1*^{mgR}, and *Efemp2*
311 SMKO) and elsewhere (*Col3a1*^{m1Lsmi}),[12,16] we applied our read-out approach to assess the
312 hitherto unknown aortic impact of CRISPR/Cas9-engineered human-equivalent mutations in
313 mouse models of three hAD candidate genes. In humans, these three genes (*LTBP1*, *MFAP4*,
314 and *TIMP1*) are expressed at higher levels in arterial tissue than in any other tissue studied in
315 GTEx (gtexportal.org/home). LTBP1 interacts with ECM proteins, such as MFS-associated

316 FBN1, and regulates transforming growth factor (TGF)-β,[47] which plays an important role in
317 the pathogenesis of hADs.[48] MFAP4, an ECM protein found in elastic fibers, actively
318 promotes tropoelastin self-assembly by binding tropoelastin and interacts with FBN1, FBN2,
319 and type I collagen.[49] TIMP1 is a strong inhibitor of many MMPs except for some of the
320 membrane type MMPs, thereby preventing excessive ECM degradation.[50] Knock-out mouse
321 models of *Ltbp1*, *Mfap4*, and *Timp1* showed cardiovascular phenotypes,[51-56] indicating that
322 mutations in these genes could be causative for hAD.

323 In contrast to established hAD mouse models (i.e., mice with mutation in the genes
324 *Fbn1*, *Efemp2*, or *Col3a1*), however, our read-out system revealed no significantly reduced
325 aortic rupture force for any genotypes of the three novel knock-in mouse models $Ltbp1^{G1132S}$,
326 $Mfap4^{D42A}$, and $Timp1^{I120T}$ at the age of 1 year (Figure 5). This indicates and clarifies the lack
327 of aortic significance of the sequence variants with unknown pathogenicity knocked into our
328 mouse models. The non-reduced aortic rupture force of the three knock-in mouse models are
329 consistent with their non-reduced survival rate (data not shown). It is important to note,
330 however, that survival rate does not reflect aortic rupture force at the individual level, as not
331 all mice with significantly reduced rupture force have a reduced survival.[16] Further studies are
332 needed to assess the clinical significance of the genes *LTBP1*, *MFAP4*, and *TIMP1* in hAD,
333 also considering a disease-modifying (synergistic) effect of these genes as well as mice with a
334 different genetic background.

335 Indeed, although mice can well model human diseases (*in vivo*) as demonstrated here
336 for hAD, mouse models cannot always accurately mimic human disease phenotypes.[57] For
337 example, the X-linked *BGN* gene encoding biglycan, which is already associated with hAD in
338 humans,[58] has been shown not to cause an aortic phenotype when *Bgn* is knocked out on the
339 C57BL/6 mouse background (likely due to the relative deficiency of TGF-β signaling induced
340 by the C57BL/6 background),[59] whereas biglycan deficiency in male BALB/cA mice leads to
341 sudden death due to aortic rupture.[60]

342 Taken together, this study demonstrates that our read-out system of aortic rupture
343 force can not only explain the aortic phenotype of established mouse hAD models but also
344 clarify the unknown/uncertain aortic significance of candidate genes, variants, and drugs,
345 thereby paving the way for better molecular diagnosis and medical therapies in hAD. Thus, it
346 is obvious that comprehensive studies related to aortic aneurysms, dissections, and ruptures
347 should consider and assess the biomechanical integrity (rupture force) of the aortic wall.
348

349 **Acknowledgements**
350 We thank Cyagen (Santa Clara, CA, USA) for help with the generation of the three
351 CRISPR/Cas9 knock-in mouse models, Bryana M. Levitan for performing ultrasound
352 measurements of *Fbn1*^{mgR} mice as well as Daniela Brkan, Edina Jusufi, Marc T. Schönholzer,
353 Giancarlo Tomio, and Dzenneta Zukovic for help with data analysis and/or figure preparation.
354

355 **Sources of Funding**
356 This work was supported by the Isaac Dreyfus-Bernheim Stiftung and the Fondation pour la
357 Recherche et le Traitement Médical (FRTM) as well as by NIH NHLBI (grant number K01
358 HL149984) and JSPS KAKENHI (grant number JP20H03762).
359

360 **Disclosures**
361 None.
362

363 **Supplemental Material**
364 Statistical Analyses
365 Figures S1 and S2
366 Tables S1-S12
367 Major Resources Table
368

369 **REFERENCES**

370 1. Lindsay ME, Dietz HC. Lessons on the pathogenesis of aneurysm from heritable
371 conditions. *Nature*. 2011;473:308-316. doi: 10.1038/nature10145
372 2. Verstraeten A, Luyckx I, Loeys B. Aetiology and management of hereditary aortopathy.
373 *Nat Rev Cardiol*. 2017;14:197-208. doi: 10.1038/nrcardio.2016.211
374 3. Creamer TJ, Bramel EE, MacFarlane EG. Insights on the pathogenesis of aneurysm
375 through the study of hereditary aortopathies. *Genes*. 2021;12:183. doi:
376 10.3390/genes12020183
377 4. Caspar SM, Dubacher N, Kopps AM, Meienberg J, Henggeler C, Matyas G. Clinical
378 sequencing: From raw data to diagnosis with lifetime value. *Clin Genet*. 2018;93:508-
379 519. doi: 10.1111/cge.13190
380 5. Renard M, Francis C, Ghosh R, Scott AF, Witmer PD, Adès LC, Andelfinger GU,
381 Arnaud P, Boileau C, Callewaert BL, Guo D, Hanna N, Lindsay ME, Morisaki H,
382 Morisaki T, Pachter N, Robert L, Van Laer L, Dietz HC, Loeys BL, Milewicz DM, De
383 Backer J. Clinical Validity of Genes for Heritable Thoracic Aortic Aneurysm and
384 Dissection. *J Am Coll Cardiol*. 2018;72:605-615. doi: 10.1016/j.jacc.2018.04.089
385 6. Caspar SM, Dubacher N, Matyas G. More Genes for Thoracic Aortic Aneurysms and
386 Dissections. *J Am Coll Cardiol*. 2019;73:528-529. doi: 10.1016/j.jacc.2018.09.094
387 7. Humphrey JD, Milewicz DM, Tellides G, Schwartz MA. Dysfunctional mechanosensing
388 in aneurysms. *Science*. 2014;344:477-479. doi: 10.1126/science.1253026
389 8. Humphrey JD, Schwartz MA, Tellides G, Milewicz DM. Role of mechanotransduction in
390 vascular biology: focus on thoracic aortic aneurysms and dissections. *Circ Res*.
391 2015;116:1448-1461. doi: 10.1161/CIRCRESAHA.114.304936
392 9. Pierce DM, Maier F, Weisbecker H, Viertler C, Verbrugghe P, Famaey N, Fourneau I,
393 Herijgers P, Holzapfel GA. Human thoracic and abdominal aortic aneurysmal tissues:

Damage experiments, statistical analysis and constitutive modeling. *J Mech Behav Biomed Mater*. 2015;41:92-107. doi: 10.1016/j.jmbbm.2014.10.003

10. Chiu P, Lee H-P, Dalal AR, Koyano T, Nguyen M, Connolly AJ, Chaudhuri O, Fischbein MP. Relative strain is a novel predictor of aneurysmal degeneration of the thoracic aorta: An ex vivo mechanical study. *JVS Vasc Sci*. 2021;2:235-246. doi: 10.1016/j.jvssci.2021.08.003
11. Chittajallu SNSH, Richhariya A, Tse KM, Chinthapenta V. A Review on Damage and Rupture Modelling for Soft Tissues. *Bioengineering (Basel)*. 2022;9:26. doi: 10.3390/bioengineering9010026
12. Dubacher N, Münger J, Gorosabel MC, Crabb J, Ksiazek AA, Caspar SM, Bakker ENTP, van Bavel E, Ziegler U, Carrel T, Steinmann B, Zeisberger S, Meienberg J, Matyas G. Celiprolol but not losartan improves the biomechanical integrity of the aorta in a mouse model of vascular Ehlers-Danlos syndrome. *Cardiovasc Res*. 2019;16:457-465. doi: 10.21037/acs.2017.11.10
13. Ong K-T, Perdu J, De Backer J, Bozec E, Collignon P, Emmerich J, Fauret A-L, Fiessinger J-N, Germain DP, Georgesco G, Hulot J-S, De Paepe A, Plauchu H, Jeunemaitre X, Laurent S, Boutouyrie P. Effect of celiprolol on prevention of cardiovascular events in vascular Ehlers-Danlos syndrome: a prospective randomised, open, blinded-endpoints trial. *Lancet* 2010;376:1476-1484. doi: 10.1016/S0140-6736(10)60960-9
14. Frank M, Adham S, Seigle S, Legrand A, Mirault T, Henneton P, Albuisson J, Denarié N, Mazzella J-M, Mousseaux E, Messas E, Boutouyrie P, Jeunemaitre X. Vascular Ehlers-Danlos Syndrome: Long-Term Observational study. *J Am Coll Cardiol.* 2019;73:1948-1957. doi: 10.1016/j.jacc.2019.01.058

418 15. Baderkhan H, Wanhainen A, Stenborg A, Stattin E-L, Björck M. Celiprolol Treatment in
419 Patients with Vascular Ehlers-Danlos Syndrome. *Eur J Vasc Endovasc Surg.*
420 2021;61:326-331. doi: 10.1016/j.ejvs.2020.10.020
421 16. Gorosabel MC, Dubacher N, Meienberg J, Matyas G. Vascular Ehlers-Danlos syndrome:
422 can the beneficial effect of celiprolol be extrapolated to bisoprolol? *EHJ - Cardiovasc*
423 *Pharmacother*. 2020;6:199-200. doi: 10.1093/ehjcvp/pvz067
424 17. Judge DP, Biery NJ, Keene DR, Geubtner J, Myers L, Huso DL, Sakai LY, Dietz HC.
425 Evidence for a critical contribution of haploinsufficiency in the complex pathogenesis of
426 Marfan syndrome. *J Clin Invest*. 2004;114:172-181. doi: 10.1172/JCI20641
427 18. Pereira L, Lee SY, Gayraud B, Andrikopoulos K, Shapiro SD, Bunton T, Biery NJ, Dietz
428 HC, Sakai LY, Ramirez F. Pathogenetic sequence for aneurysm revealed in mice
429 underexpressing fibrillin-1. *Procl Natl Acad Sci U S A*. 1999;96:3819-3823. doi:
430 10.1073/pnas.96.7.3819
431 19. Bunton TE, Biery NJ, Myers L, Gayraud B, Ramirez F, Dietz HC. Phenotypic Alteration
432 of Vascular Smooth Muscle Cells Precedes Elastolysis in a Mouse Model of Marfan
433 Syndrome. *Circ Res*. 2001;88:37-43. doi: 10.1161/01.res.88.1.37
434 20. Saeyeldin A, Zafar MA, Velasquez CA, Ip K, Gryaznov A, Brownstein AJ, Li Y, Rizzo
435 JA, Erben Y, Ziganshin BA, Elefteriades JA. Natural history of aortic root aneurysms in
436 Marfan syndrome. *Ann Cardiothorac Surg*. 2017;6:625-632. doi:
437 10.21037/acs.2017.11.10
438 21. Habashi JP, Judge DP, Holm TM, Cohn RD, Loeys BL, Cooper TK, Myers L, Klein EC,
439 Liu G, Calvi C, Podowski M, Neptune ER, Halushka MK, Bedja D, Gabrielson K, Rifkin
440 DB, Carta L, Ramirez F, Huso DL, Dietz HC. Losartan, an AT1 Antagonist, Prevents
441 Aortic Aneurysm in a Mouse Model of Marfan Syndrome. *Science*. 2006;312:117-121.
442 doi: 10.1681/ASN.2006050508

443 22. Habashi JP, Doyle JJ, Holm TM, Aziz H, Schoenhoff F, Bedja D, Chen Y, Modiri AN,
444 Judge DP, Dietz HC. Angiotensin II Type 2 Receptor Signaling Attenuates Aortic
445 Aneurysm in Mice Through ERK Antagonism. *Science*. 2011;332:361-365. doi:
446 10.1126/science.1192152
447 23. Bhatt AB, Buck JS, Zuflacht JP, Milian J, Kadivar S, Gauvreau K, Singh MN, Creager
448 MA. Distinct effects of losartan and atenolol on vascular stiffness in Marfan syndrome.
449 *Vasc Med*. 2015;20:317-325. doi: 10.1177/1358863X15569868
450 24. Cook JR, Clayton NP, Carta L, Galatioto J, Chiu E, Smaldone S, Nelson CA, Cheng SH,
451 Wentworth BM, Ramirez F. Dimorphic effects of transforming growth factor-β signaling
452 during aortic aneurysm progression in mice suggest a combinatorial therapy for Marfan
453 syndrome. *Arterioscler Thromb Vasc Biol*. 2015;35:911-917. doi:
454 10.1161/ATVBAHA.114.305150
455 25. Sellers SL, Milad N, Chan R, Mielnik M, Jermilova U, Huang PL, Crom R de, Hirota JA,
456 Hogg JC, Sandor GG, Van Breemen C, Esfandiarei M, Seidman MA, Bernatchez P.
457 Inhibition of Marfan Syndrome Aortic Root Dilation by Losartan: Role of Angiotensin II
458 Receptor Type 1-Independent Activation of Endothelial Function. *Am J Pathol*.
459 2018;188:574-585. doi: 10.1016/j.ajpath.2017.11.006
460 26. Huang J, Davis EC, Chapman SL, Budatha M, Marmorstein LY, Word RA, Yanagisawa
461 H. Fibulin-4 Deficiency Results in Ascending Aortic Aneurysms: A Potential Link
462 Between Abnormal Smooth Muscle Cell Phenotype and Aneurysm Progression. *Circ Res*.
463 2010;106:583-592. doi: 10.1161/CIRCRESAHA.109.207852
464 27. Hucthagowder V, Sausgruber N, Kim KH, Angle B, Marmorstein LY, Urban Z. Fibulin-
465 4: A Novel Gene for an Autosomal Recessive Cutis Laxa Syndrome. *Am J Hum Genet*.
466 2006;78:1075-1080. doi: 10.1086/504304
467 28. Renard M, Holm T, Veith R, Callewaert BL, Adès LC, Baspinar O, Pickart A, Dasouki
468 M, Hoyer J, Rauch A, Trapane P, Earing MG, Coucke PJ, Sakai LY, Dietz HC, De Paepe

469 AM, Loeys BL. Altered TGFβ signaling and cardiovascular manifestations in patients
470 with autosomal recessive cutis laxa type I caused by fibulin-4 deficiency. *Eur J Hum*
471 *Genet*. 2010;18:895-901. doi: 10.1038/ejhg.2010.45
472 29. Lee VS, Halabi CM, Hoffman EP, Carmichael N, Leshchiner I, Lian CG, Bierhals AJ,
473 Vuzman D, Brigham Genomic Medicine, Mecham RP, Frank NY, Stitziel NO. Loss of
474 function mutation in *LOX* causes thoracic aortic aneurysm and dissection in humans. *Proc*
475 *Natl Acad Sci U S A*. 2016;113:8759-8764. doi: 10.1073/pnas.1601442113
476 30. Halabi CM, Broekelmann TJ, Lin M, Lee VS, Chu M-L, Mecham RP. Fibulin-4 is
477 essential for maintaining arterial wall integrity in conduit but not muscular arteries. *Sci*
478 *Adv*. 2017;3:e1602532. doi: 10.1126/sciadv.1602532
479 31. Parker SJ, Stotland A, MacFarlane E, Wilson N, Orosco A, Venkatraman V, Madrid K,
480 Gottlieb R, Dietz HC, Van Eyk JE. Proteomics reveals Rictor as a noncanonical TGF-β
481 signaling target during aneurysm progression in Marfan mice. *Am J Physiol Heart Circ*
482 *Physiol*. 2018;315:H1112-H1126. doi: 10.1152/ajpheart.00089.2018
483 32. Bhushan R, Altinbas L, Jäger M, Zaradzki M, Lehmann D, Timmermann B, Clayton NP,
484 Zhu Y, Kallenbach K, Kararigas G, Robinson PN. An integrative systems approach
485 identifies novel candidates in Marfan syndrome-related pathophysiology. *J Cell Mol Med*.
486 2019;23:2526-2535. doi: 10.1111/jcmm.14137
487 33. Bowen CJ, Calderón Giadrosic JF, Burger Z, Rykiel G, Davis EC, Helmers MR, Benke
488 K, Gallo MacFarlane E, Dietz HC. Targetable cellular signaling events mediate vascular
489 pathology in vascular Ehlers-Danlos syndrome. *J Clin Invest*. 2020;130:686-698. doi:
490 10.1172/JCI130730
491 34. Xiong W, Meisinger T, Knispel R, Worth JM, Baxter BT. MMP-2 Regulates Erk1/2
492 Phosphorylation and Aortic Dilatation in Marfan Syndrome. *Circ Res*. 2012;110:e92-
493 e101. doi: 10.1161/CIRCRESAHA.112.268268

494 35. Sheppard MB, Chen JZ, Rateri DL, Moorleghen JJ, Weiland M, Daugherty A. Renin-
495 Angiotensin System Inhibitors Do Not Improve Survival in Fibrillin-1 Hypomorphic
496 Mice with Established Aortic Aneurysm. *J Clin Trans Sci*. 2019;3:112-113. doi:
497 10.1017/cts.2019.258
498 36. Muthu ML, Tiedemann K, Fradette J, Komarova S, Reinhardt DP. Fibrillin-1 regulates
499 white adipose tissue development, homeostasis, and function. *Matrix Biol*.
500 2022;110:106-128. doi: 10.1016/j.matbio.2022.05.002
501 37. Chen JZ, Rateri D, Sheppard M, Daugherty A. Abstract 20315: Sexual Dimorphism in a
502 Marfan Syndrome Mouse Model. *Circulation*. 2017;136:A20315.
503 38. Chen JZ, Sawada H, Moorleghen JJ, Weiland M, Daugherty A, Sheppard MB. Aortic
504 Strain Correlates With Elastin Fragmentation in Fibrillin-1 Hypomorphic Mice. *Circ Rep*.
505 2019;1:199-205. doi: 10.1253/circrep.CR-18-0012
506 39. Détaint D, Faivre L, Collod-Beroud G, Child AH, Loeys BL, Binquet C, Gautier E,
507 Arbustini E, Mayer K, Arslan-Kirchner M, Stheneur C, Halliday D, Beroud C, Bonithon-
508 Kopp C, Claustres M, Plauchu H, Robinson PN, Kiotsekoglou A, De Backer J, Adès L,
509 Francke U, De Paepe A, Boileau C, Jondeau G. Cardiovascular manifestations in men and
510 women carrying a FBN1 mutation. *Eur Heart J*. 2010;31:2223-2229. doi:
511 10.1093/eurheartj/ehq258
512 40. Holmes KW, Maslen CL, Kindem M, Kroner BL, Song HK, Ravekes W, Dietz HC,
513 Weinsaft JW, Roman MJ, Devereux RB, Pyeritz RE, Bavaria J, Milewski K, Milewicz D,
514 LeMaire SA, Hendershot T, Eagle KA, Tolunay HE, Desvigne-Nickens P, Silberbach M,
515 for the GenTAC Registry Consortium. GenTAC registry report: Gender differences
516 among individuals with genetically triggered thoracic aortic aneurysm and dissection. *Am*
517 *J Med Genet*. 2013;161:779-786. doi: 10.1002/ajmg.a.35836

518 41. Renard M, Muiño-Mosquera L, Manalo EC, Tufa S, Carlson EJ, Keene DR, De Backer J,
519 Sakai LY. Sex, pregnancy and aortic disease in Marfan syndrome. *PLoS ONE*.
520 2017;12:e0181166. doi: 10.1371/journal.pone.0181166
521 42. Horiguchi M, Inoue T, Ohbayashi T, Hirai M, Noda K, Marmorstein LY, Yabe D, Takagi
522 K, Akama TO, Kita T, Kimura T, Nakamura T. Fibulin-4 conducts proper elastogenesis
523 via interaction with cross-linking enzyme lysyl oxidase. *Proc Natl Acad Sci U S A*.
524 2009;106:19029-19034. doi: 10.1073/pnas.0908268106
525 43. Papke CL, Yanagisawa H. Fibulin-4 and fibulin-5 in elastogenesis and beyond: Insights
526 from mouse and human studies. *Matrix Biol*. 2014;37:142-149. doi:
527 10.1016/j.matbio.2014.02.004
528 44. Papke CL, Tsunezumi J, Ringuette L-J, Nagaoka H, Terajima M, Yamashiro Y, Urquhart
529 G, Yamauchi M, Davis EC, Yanagisawa H. Loss of fibulin-4 disrupts collagen synthesis
530 and maturation: implications for pathology resulting from *EFEMP2* mutations. *Hum Mol*
531 *Genet*. 2015;24:5867-5879. doi: 10.1093/hmg/ddv308
532 45. Ruddy JM, Jones JA, Spinale FG, Ikonomidis JS. Regional heterogeneity within the
533 aorta: Relevance to aneurysm disease. *J Thorac Cardiovasc Surg*. 2008;136:1123-1130.
534 doi: 10.1016/j.jtcvs.2008.06.027
535 46. Jana S, Hu M, Shen M, Kassiri Z. Extracellular matrix, regional heterogeneity of the
536 aorta, and aortic aneurysm. *Exp Mol Med*. 2019;51:1-15. doi: 10.1038/s12276-019-0286-3
537 47. Morisaki T, Morisaki H. Genetics of hereditary large vessel diseases. *J Hum Genet*.
538 2016;61:21-26. doi: 10.1038/jhg.2015.119
539 48. Neptune ER, Frischmeyer PA, Arking DE, Myers L, Bunton TE, Gayraud B, Ramirez F,
540 Sakai LY, Dietz HC. Dysregulation of TGF-β activation contributes to pathogenesis in
541 Marfan syndrome. *Nat Genet*. 2003;33:407-411. doi: 10.1038/ng1116
542 49. Pilecki B, Holm AT, Schlosser A, Moeller JB, Wohl AP, Zuk AV, Heumüller SE, Wallis
543 R, Moestrup SK, Sengle G, Holmskov U, Sorensen GL. Characterization of

544 Microfibrillar-associated Protein 4 (MFAP4) as a Tropoelastin- and Fibrillin-binding
545 Protein Involved in Elastic Fiber Formation. *J Biol Chem*. 2016;291:1103-1114. doi:
546 10.1074/jbc.M115.681775
547 50. Brew K, Nagase H. The tissue inhibitors of metalloproteinases (TIMPs): An ancient
548 family with structural and functional diversity. *Biochim Biophys Acta*. 2010;1803:55-71.
549 doi: 10.1016/j.bbamcr.2010.01.003
550 51. Roten L, Nemoto S, Simsic J, Coker ML, Rao V, Baicu S, Defreyte G, Soloway PJ, Zile
551 MR, Spinale FG. Effects of Gene Deletion of the Tissue Inhibitor of the Matrix
552 Metalloproteinase-type 1 (TIMP-1) on Left Ventricular Geometry and Function in Mice.
553 *J Mol Cell Cardiol*. 2000;32:109-120. doi: 10.1006/jmcc.1999.1052
554 52. Eskandari MK, Vijungco JD, Flores A, Borensztajn J, Shively V, Pearce WH. Enhanced
555 abdominal aortic aneurysm in TIMP-1-deficient mice. *J Surg Res*. 2005;123:289-293. doi:
556 10.1016/j.jss.2004.07.247
557 53. Todorovic V, Frendewey D, Gutstein DE, Chen Y, Freyer L, Finnegan E, Liu F, Murphy
558 A, Valenzuela D, Yancopoulos G, Rifkin DB. Long form of latent TGF-β binding protein
559 1 (Ltbp1L) is essential for cardiac outflow tract septation and remodeling. *Development*.
560 2007;134:3723-3732. doi: 10.1242/dev.008599
561 54. Todorovic V, Finnegan E, Freyer L, Zilberberg L, Ota M, Rifkin DB. Long form of latent
562 TGF-β binding protein 1 (Ltbp1L) regulates cardiac valve development. *Dev Dyn*.
563 2011;240:176-187. doi: 10.1002/dvdy.22521
564 55. Schlosser A, Pilecki B, Hemstra LE, Kejling K, Kristmannsdottir GB, Wulf-Johansson H,
565 Moeller JB, Füchtbauer E-M, Nielsen O, Kirketerp-Møller K, Dubey LK, Hansen PBL,
566 Stubbe J, Wrede C, Hegermann J, Ochs M, Rathkolb B, Schrewe A, Bekeredjian R, Wolf
567 E, Gailus-Durner V, Fuchs H, Hrabě de Angelis M, Lindholt JS, Holmskov U, Sorensen
568 GL. MFAP4 Promotes Vascular Smooth Muscle Migration, Proliferation and Accelerates

569 Neointima Formation. *Arterioscler Thromb Vasc Biol*. 2016;36:122-133. doi:
570 10.1161/ATVBAHA.115.306672
571 56. Arpino V, Brock M, Gill SE. The role of TIMPs in regulation of extracellular matrix
572 proteolysis. *Matrix Biol*. 2015;44-46:247-254. doi: 10.1016/j.matbio.2015.03.005
573 57. Ritskes-Hoitinga M, Leenaars C, Beumer W, Coenen-de Roo T, Stafleu F, Meijboom
574 FLB. Improving Translation by Identifying Evidence for More Human-Relevant
575 Preclinical Strategies. *Animals*. 2020;10:1170. doi: 10.3390/ani10071170
576 58. Meester JAN, Vandeweyer G, Pintelon I, Lammens M, Van Hoorick L, De Belder S,
577 Waitzman K, Young L, Markham LW, Vogt J, Richer J, Beauchesne LM, Unger S,
578 Superti-Furga A, Prsa M, Dhillon R, Reyniers E, Dietz HC, Wuyts W, Mortier G,
579 Verstraeten A, Van Laer L, Loeys BL. Loss-of-function mutations in the X-linked
580 biglycan gene cause a severe syndromic form of thoracic aortic aneurysms and
581 dissections. *Genet Med*. 2017;19:386-395. doi: 10.1038/gim.2016.126
582 59. Tang T, Thompson JC, Wilson PG, Nelson C, Williams KJ, Tannock LR. Decreased
583 Body Fat, Elevated Plasma Transforming Growth Factor-β Levels, and Impaired BMP4-
584 Like Signaling in Biglycan-Deficient Mice. *Connect Tissue Res*. 2013;54:5-13. doi:
585 10.3109/03008207.2012.715700
586 60. Heegaard A-M, Corsi A, Danielsen CC, Nielsen KL, Jorgensen HL, Riminucci M, Young
587 MF, Bianco P. Biglycan Deficiency Causes Spontaneous Aortic Dissection and Rupture in
588 Mice. *Circulation*. 2007;115:2731-2738. doi: 10.1161/CIRCULATIONAHA.106.653980
589

590 **Highlights**

591 • Assay to measure the aortic rupture force as read-out for the biomechanical integrity
592 identified weakened murine thoracic aorta prior to micro- and macroscopic changes in
593 *Fbn1*$^{+/C1041G}$ mice.

594 • Despite reducing aneurysm growth, losartan treatment did not have any impact on the
595 aortic rupture force of *Fbn1*$^{mgR/mgR}$ mice.

596 • Smooth-muscle-cell-knock-out of *Efemp2* significantly impaired the rupture force of
597 the murine thoracic aorta.

598 • Aortic rupture force measurements could clarify the causality of novel candidate
599 gene(s)/variant(s) in mouse models of aortic diseases.

Graphical Abstract

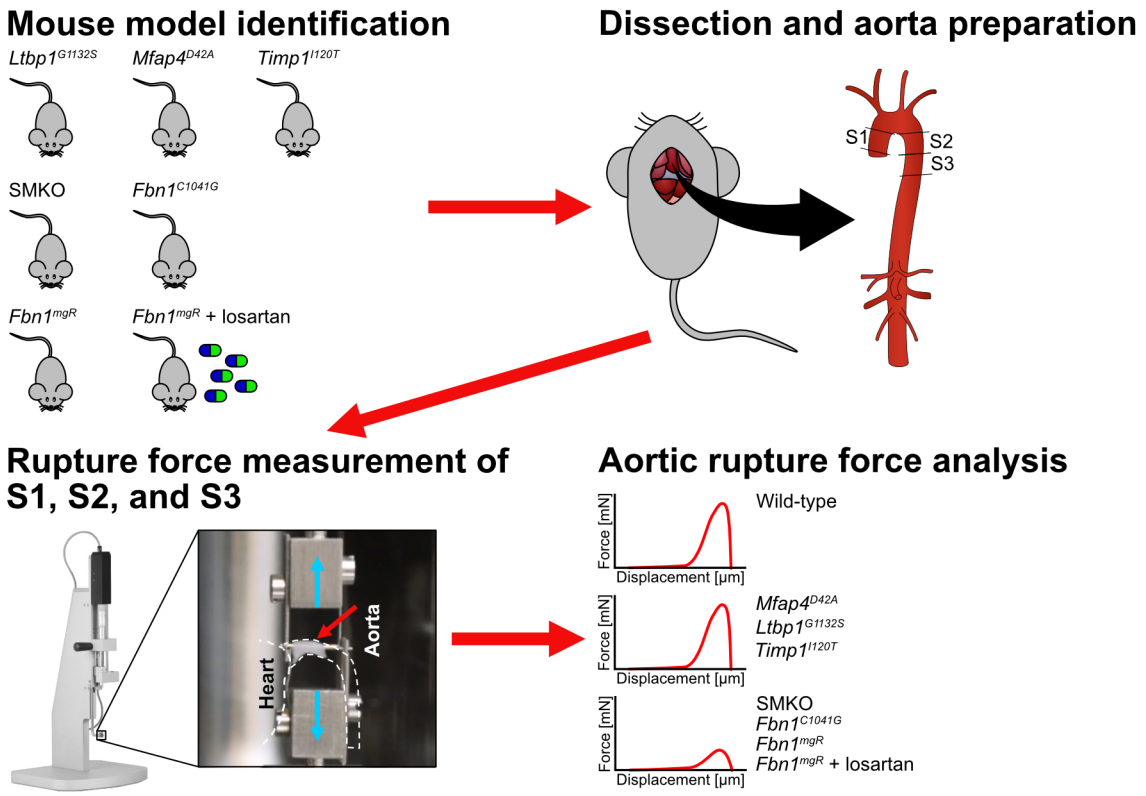

Figures and Figure Legends

Figure 1

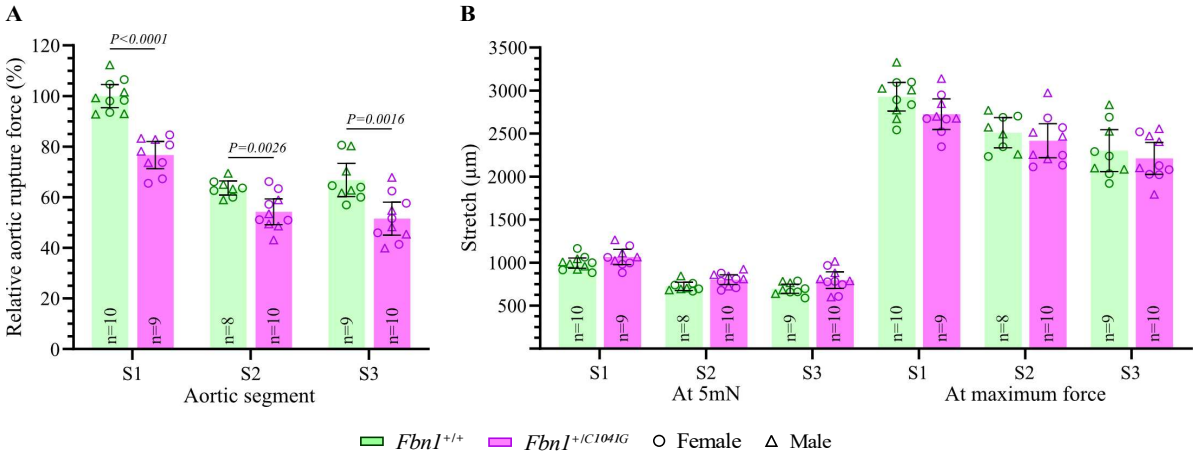

Figure 1. Aortic parameters of the *Fbn1*^{C1041G} mouse model.
A, Relative aortic rupture force (%) of three aortic segments (S1-S3) of 10-week-old *Fbn1*$^{+/+}$ and *Fbn1*$^{+/C1041G}$ mice. **B**, Stretch (in µm) of aortic segments at 5mN (load-free aortic diameter) and maximum force of 10-week-old *Fbn1*$^{+/+}$ and *Fbn1*$^{+/C1041G}$ mice. Bars represent arithmetic means and error bars indicate 95% confidence intervals. The sample size (n) is displayed (damaged segments and outliers, i.e. >2× standard deviation, were excluded). For mean values with non- or slightly overlapping 95% CIs compared in text, two-tailed *P* values of unpaired t-tests are shown (applies to **A** only).

Figure 2

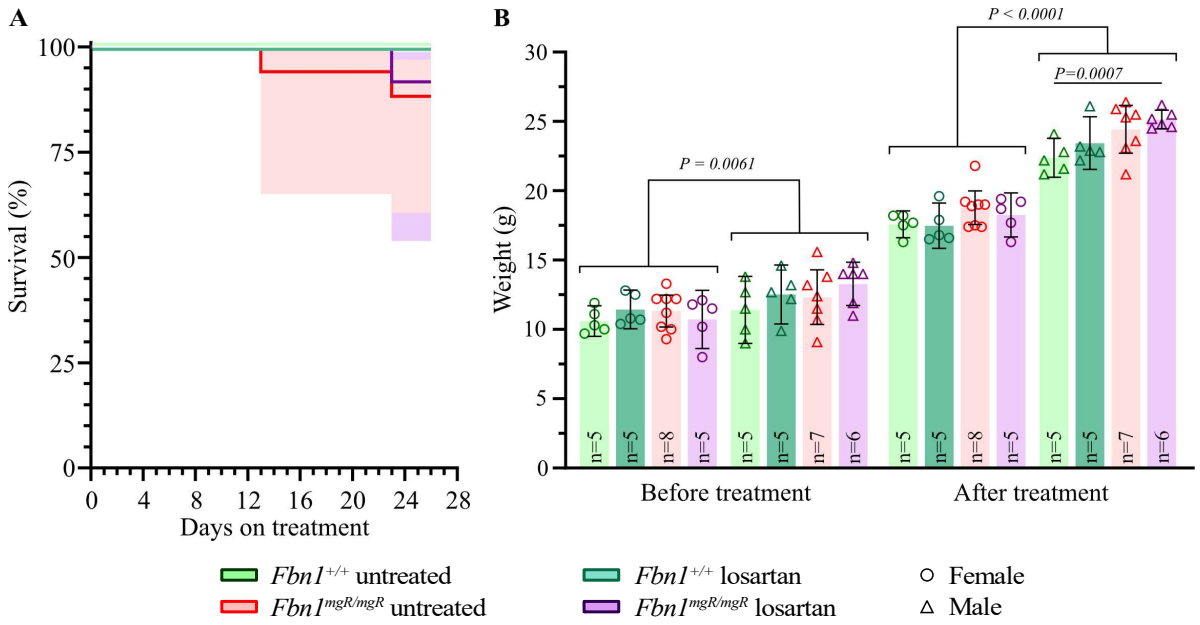

Figure 2. Survival and bodyweight of the *Fbn1*^{mgR} mouse model treated with the AGTR1-inhibitor losartan. **A**, Kaplan-Meier curve for the survival of untreated *Fbn1*$^{+/+}$ mice (n=10) and *Fbn1*$^{mgR/mgR}$ mice (n=17), and *Fbn1*$^{+/+}$ (n=10) and *Fbn1*$^{mgR/mgR}$ (n=12) mice receiving losartan between the age of 4 and 8 weeks. Note that the survival curve of losartan-treated *Fbn1*$^{+/+}$ mice is masked by that of untreated *Fbn1*$^{+/+}$ mice. 95% confidence intervals (shaded areas) are shown for *Fbn1*$^{mgR/mgR}$ mice with survivals differing from 100%. **B**, Bodyweights of mice surviving the treatment period of 4 weeks measured before and after treatment at the age of 4 and 8 weeks, respectively. Bars represent arithmetic means, error bars indicate 95% confidence intervals. Significant two-tailed *P* values of unpaired t-tests are shown ($P<0.05$). For the comparison between female and male mice (B), the respective groups were pooled prior to *P* value calculation.

Figure 3

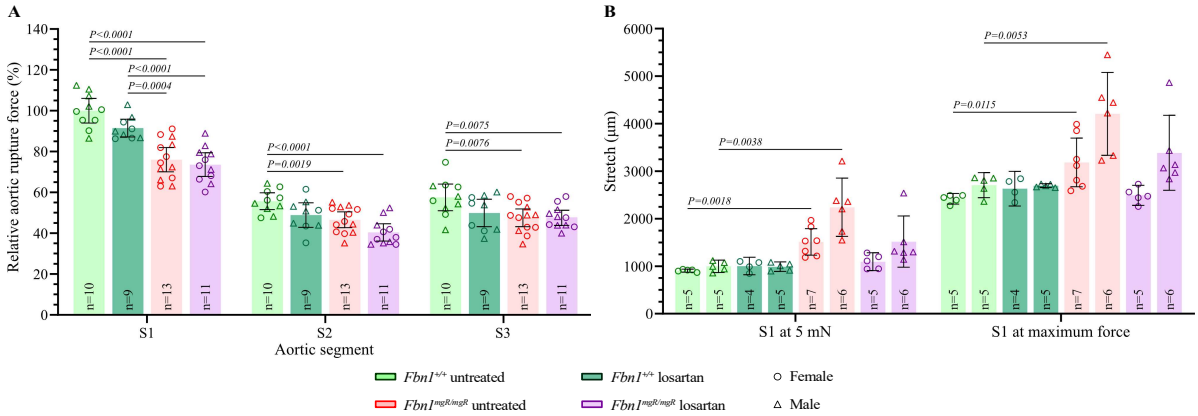

Figure 3. Aortic parameters of the *Fbn1*^{mgR} mouse model treated with the AGTR1-inhibitor losartan.
A, Relative aortic rupture force (%) of three aortic segments (S1-S3) of 8-week-old *Fbn1*$^{+/+}$ and *Fbn1*$^{mgR/mgR}$ mice after 4-week-long treatment with losartan. Untreated *Fbn1*$^{+/+}$ and *Fbn1*$^{mgR/mgR}$ mice served as control. **B**, Stretch (in µm) of the aortic segment S1 at 5 mN (load-free aortic diameter) as well as at maximum force in losartan-treated and untreated *Fbn1*$^{+/+}$ and *Fbn1*$^{mgR/mgR}$ mice separated according to sex. Bars represent arithmetic means and error bars indicate 95% confidence intervals (95% CI). The sample size (n) is displayed (damaged segments and outliers, i.e. >2× standard deviation, were excluded). For mean values with non- or slightly overlapping 95% CIs compared in text, two-tailed *P* values of unpaired t-tests are shown.

Figure 4

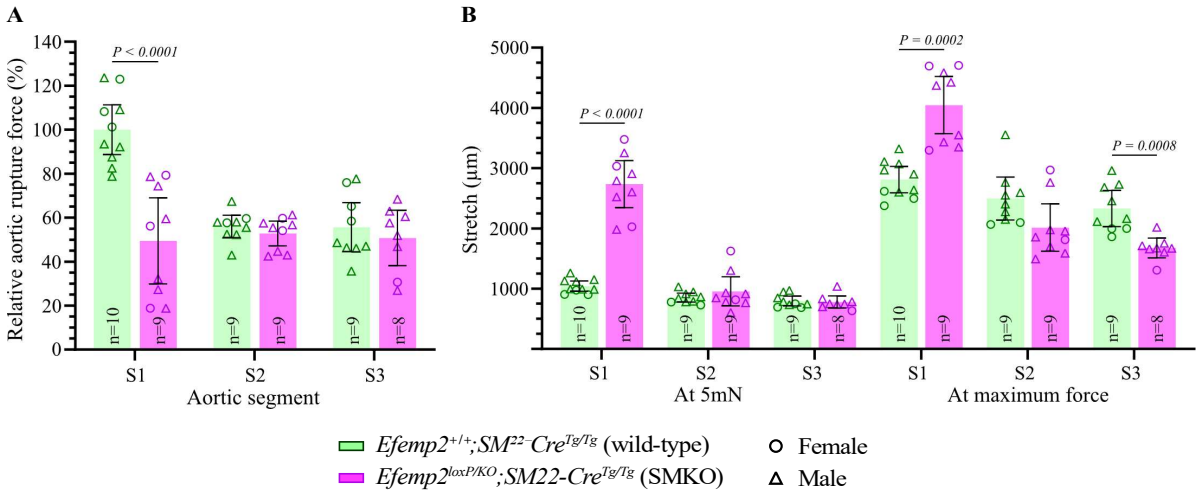

Figure 4. Aortic parameters of the *Efemp2* SMKO mouse model.
A, Relative aortic rupture force (%) of three aortic segments (S1-S3) of 8-week-old wild-type and SMKO mice. **B**, Stretch (in µm) of aortic segments at 5mN (load-free aortic diameter) as well as at maximum force in wild-type and SMKO mice. Bars represent arithmetic means and error bars indicate 95% confidence intervals. The sample size (n) is displayed (damaged segments and outliers, i.e. >2× standard deviation, were excluded). For mean values with non- or slightly overlapping 95% CIs compared in text, two-tailed *P* values of unpaired t-tests are shown.

Figure 5

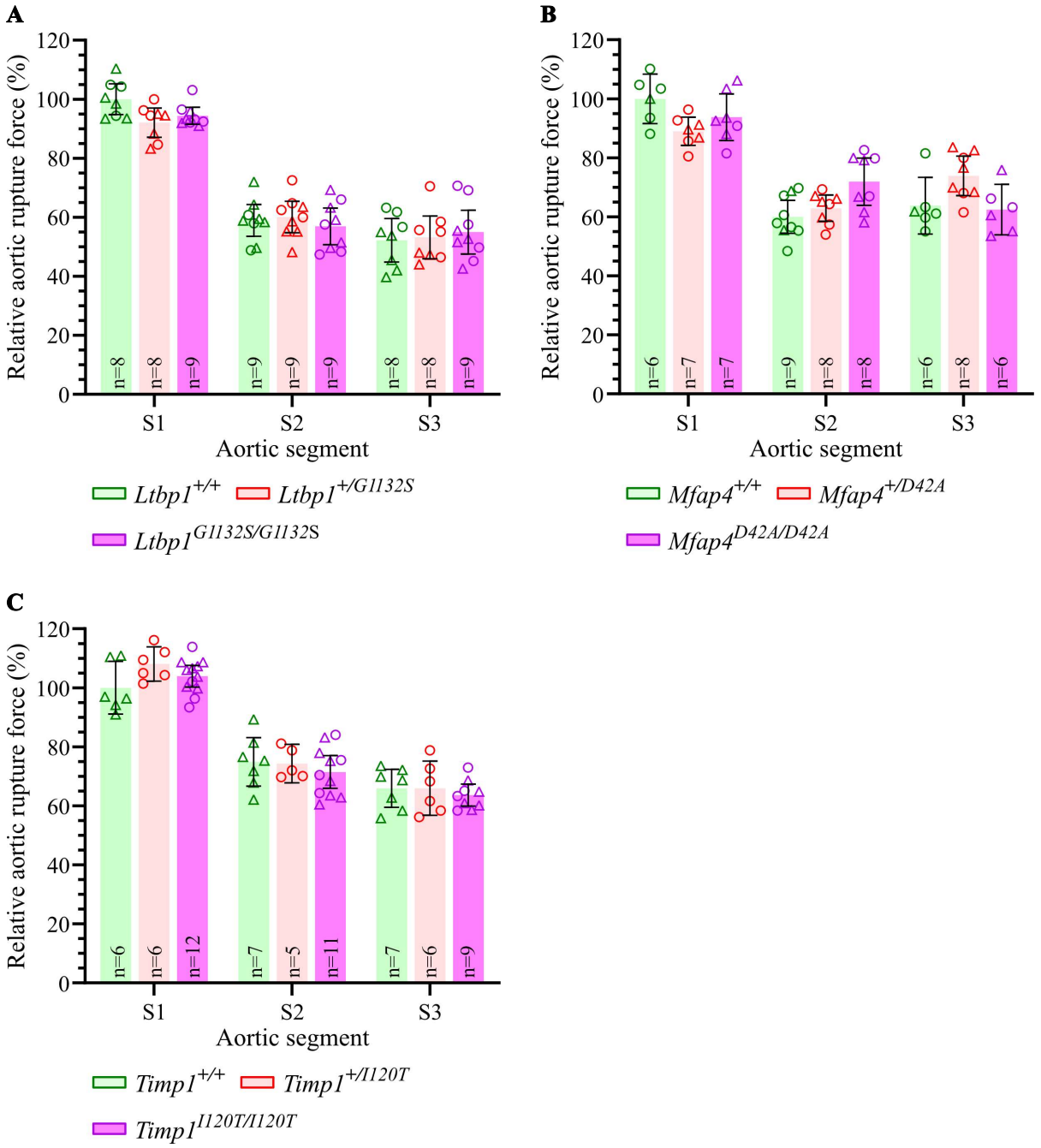

Figure 5. Aortic rupture force of the *Ltbp1*, *Mfap4*, and *Timp1* CRISPR/Cas9 knock-in mouse models.
A-C, Relative aortic rupture force (%) of three aortic segments (S1-S3) of 1-year-old wild-type and hetero- as well as hemi- and homozygous *Ltbp1* (**A**), *Mfap4* (**B**), and *Timp1* (**C**) CRISPR/Cas9 knock-in mice. Bars represent arithmetic means, error bars indicate 95% confidence intervals. The sample size (n) is displayed and damaged segments and outliers (>2× standard deviation) were excluded. Note the absence of non- or slightly overlapping 95% CIs per aortic segment. Circle, female; triangle, male.

Figure 6

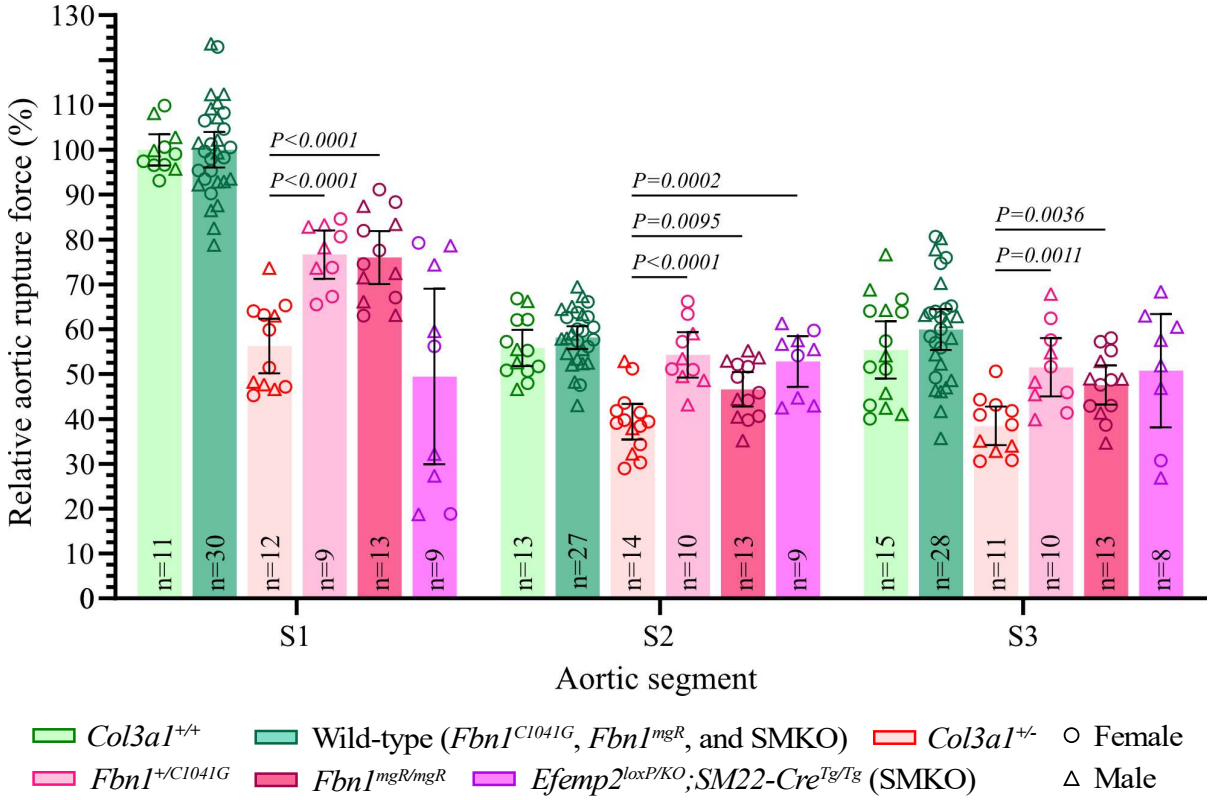

Figure 6. Aortic rupture force of the *Fbn1*^{C1041G}, *Fbn1*^{mgR}, and *Efemp2* SMKO mouse models compared to *Col3a1*^{m1Lsmi} mice modeling vEDS.

Relative aortic rupture force (%) of three aortic segments (S1-S3) of the mouse models *Col3a1*^{m1Lsmi} (data as described previously),[12] *Fbn1*^{C1041G}, *Fbn1*^{mgR}, and *Efemp2* SMKO (cf. wild-type controls of the *Fbn1*^{C1041G}, *Fbn1*^{mgR}, and *Efemp2* SMKO mouse models were pooled). Bars represent arithmetic means, error bars indicate 95% confidence intervals, The sample size (n) is displayed (damaged segments and outliers, i.e. >2× standard deviation, were excluded). For mean values with non- or slightly overlapping 95% CIs compared in text, two-tailed *P* values of unpaired t-tests are shown. *Col3a1*$^{+/+}$ and *Col3a1*$^{+/-}$ denotes wild-type and heterozygous mice of the *Col3a1*^{m1Lsmi} mouse model, respectively.